J Mater Sci: Mater Electron (2017) 28:13956–13969
DOI 10.1007/s10854-017-7245-3

Preparation of hard magnetic $BaFe_{12}O_{19}$–TiO_2 nanocomposites: applicable for photo-degradation of toxic pollutants

Zahra Ebrahimi[1] · Kambiz Hedayati[1] · Davood Ghanbari[2]

Received: 1 April 2017 / Accepted: 29 May 2017 / Published online: 2 June 2017

Abstract Barium hexa ferrite ($BaFe_{12}O_{19}$) nanoparticles were synthesized via a facile precipitation method in solvent of water. Then titanium dioxide nanoparticles as effective photo-catalyst were prepared via a simple sol–gel method. Finally $BaFe_{12}O_{19}$–TiO_2 (50:50%) nanocomposites were made by a fast chemical procedure. The effect of concentration, temperature and precipitating agent on the morphology and particle size of the products was investigated. The prepared products were characterized by X-ray diffraction, scanning electron microscopy, and Fourier transform infrared spectroscopy. Vibrating sample magnetometer shows the ferromagnetic property of the ferrite nanostructures. The photocatalytic behaviour of $BaFe_{12}O_{19}$–TiO_2 (50:50%) nanocomposites was evaluated using the degradation of azo dyes (acid black, acid violet, acid blue and methyl orange) under ultraviolet light irradiation. The results introduce a nanocomposite with applicable magnetic and photocatalytic performance.

1 Introduction

Hexagonal ferrites and their substituted derivatives have attracted considerable attention and they show very high uniaxial magnetic anisotropy so they can be used as a permanent magnetic material, which for some applications can compete technically and economically, with metallic permanent magnets [1–3]. $BaFe_{12}O_{19}$ is one of the most important hard magnetic materials, with high Curie temperature, excellent chemical stability, corrosion resistivity excellent high-frequency response and narrow switching field distribution it widely used for permanent magnets, magnetic recording, microwave absorbers. Barium ferrite is a ferromagnetic material, which has a collinear five-sublattice magnetic structure with easy axis parallel to the c-axis of the hexagonal unit cell. Its crystal structure can be divided in several blocks according to the stacking form of closely packed oxygen ions [4–6].

Alternatively, wet synthesis procedures have been developed. Usually, these procedures involve the coprecipitation of ferrihydrite, or amorphous ferric hydrous oxide, and barium hydroxide, followed by calcination to relatively low temperatures. High-frequency electromagnetic properties of the barium ferrite family have also been investigated from the view point of the application to the high-frequency active devices or electromagnetic wave absorbers [7].

Growing social concern about the impact of different chemicals on the environment has focused attention on finding ways for more effective pollution abatement methods. Following this, one of the more promising techniques is to use a photocatalytic route to oxidize such chemicals [8, 9]. The strong oxidizing power of the photo-generated holes, the chemical inertness, and the non-toxicity of TiO_2 has also made it a superior photocatalyst. This material is known to exist in several forms, among them the most abundant are anatase, rutile and brookite [8]. TiO_2 is superior than other substances because of its high photocatalytic activity and chemical stability in aqueous solution under UV light irradiation. Highly dispersed fine particles on porous support materials and suspended fluids in liquid medium. When the suspension TiO_2 is used for photodegradation of organic

✉ Kambiz Hedayati
K-hedayati@arakut.ac.ir

[1] Department of Science, Arak University of Technology, Arak, Iran

[2] Young Researchers and Elite Club, Arak Branch, Islamic Azad University, Arak, Iran

compounds, the suspended TiO_2 must be separated after each reaction. This problem could be avoided by using the TiO_2 on the magnetic cores [9].

2 Experimental

2.1 Materials and methods

$Ba(NO_3)_2$, $Fe(NO_3)_3 \cdot 9H_2O$, NaOH, NH_3 32%, tetraisopropyl orthotitanate (TTIP), polyvinylpyrrolidone, starch, gelatin, glucose, salicylic acid, nitric acid, methanol, ethanol and acetone were purchased from Merck or Aldrich and all the chemicals were used as received without further purifications. A multi-wave ultrasonic generator (Bandeline MS 73), with a converter/transducer and titanium oscillator, operating at 20 kHz with a maximum power output of 150 W was used for the ultrasonic irradiation. Room temperature magnetic properties were investigated using vibrating sample magnetometer (VSM) device, by Meghnatis Kavir Kashan Company (Iran) in an applied magnetic field sweeping between ±10,000 Oe. X-ray diffraction (XRD) patterns were recorded by a Philips, X-ray

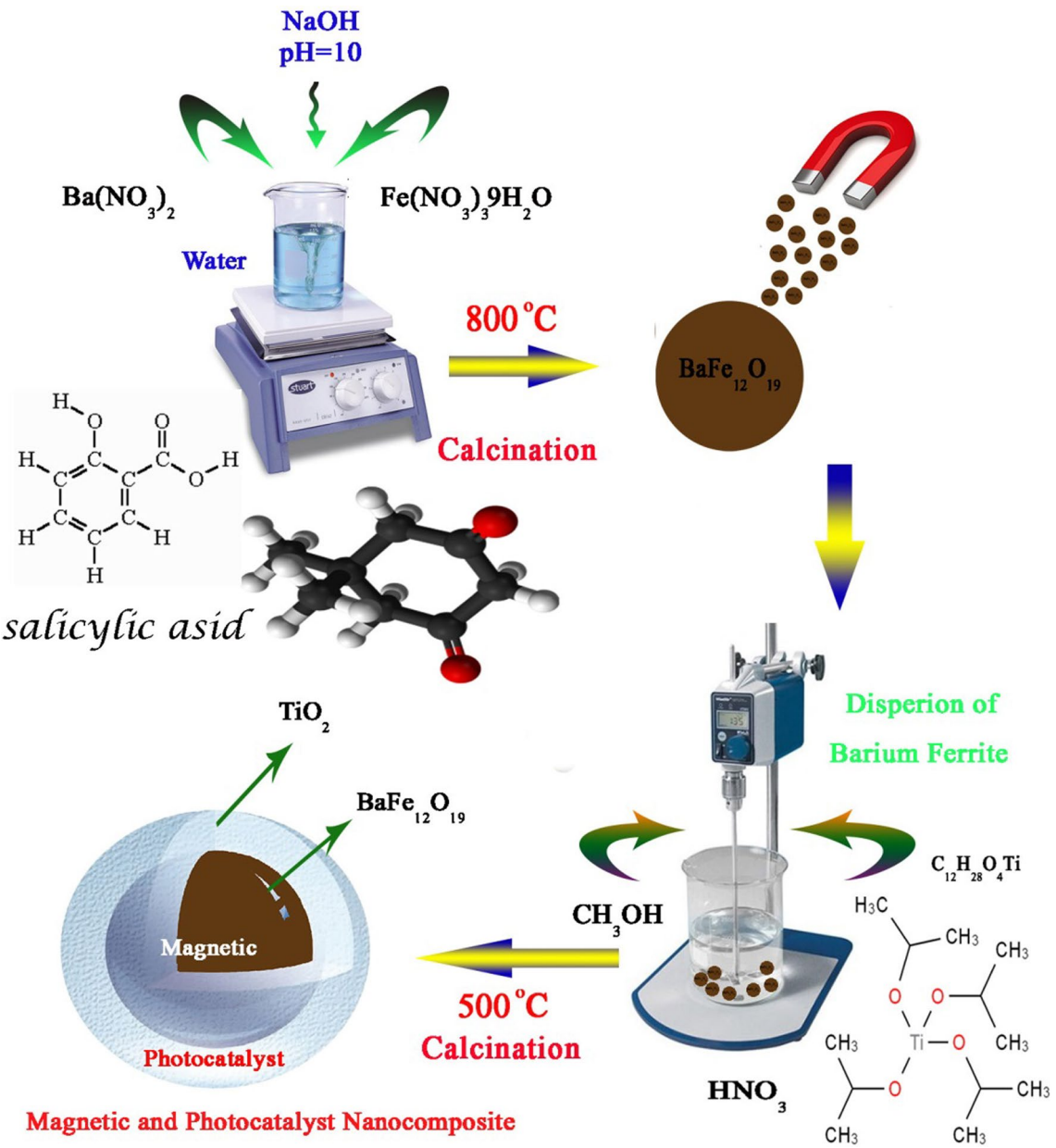

Fig. 1 Schematic of ferrite and nanocomposite preparation

diffractometer using Ni-filtered CuK_{α} radiation. Scanning electron microscopy (SEM) images were obtained using a LEO instrument model 1455VP. Prior to taking images, the samples were coated by a very thin layer of Pt (using a BAL-TEC SCD 005 sputter coater) to make the sample surface conductor and obtaining a better contrast.

2.2 Synthesis of $BaFe_{12}O_{19}$ nanoparticles

0.1 g of $Ba(NO_3)_2$ and 1.85 g of $Fe(NO_3)_3 \cdot 9H_2O$ were dissolved in 100 ml of deionized water. 30 ml of NaOH solution (1 M) was then slowly added to the solution until reaching pH to about 10. A brown precipitate was then centrifuged and washed with distilled water. Eventually the obtained precipitate was calcined at 800 °C and its color goes from brown to black. Figure 1 shows the schematic diagram for experimental setup for nanoparticle and nanocomposite preparation used in the precipitation procedure.

2.3 Synthesis of TiO_2 nanoparticles

0.25 g of TTIP was added to 10 ml of methanol. Then 1 ml of distilled water was added to the solution. In this level white sol was formed. Sol was stirred for 20 min, then 0.2 ml of HNO_3 was added to the sol until pH reaching around 2. After 90 min stirring gel was formed. Finally the obtained powder was calcined at 500 °C.

2.4 Synthesis of ($BaFe_{12}O_{19}$–TiO_2 50:50%) nanocomposite

0.1 g (50%) of $BaFe_{12}O_{19}$ was dispersed in 10 ml of methanol. Then 0.25 g of TTIP (Yield of TiO_2:0.1 g, 50%) was added to the mixture containing $BaFe_{12}O_{19}$. Then 1 ml of distilled water was added to the mixture and was stirred for 20 min. Then 0.2 ml of HNO_3 was slowly added to the aqueous solution and was stirred for 90 min, until white gel was formed. After 1 h the gel was placed in the oven (70 °C) to dry. Finally obtained powder was calcined at 500 °C.

2.5 Photo-catalytic degradation process

5 ml of the dye solution (10 ppm) was used to determine the photocatalytic activity. For degradation of 10 ml solution 0.1 g of catalyst was used. The solution was irradiated under UV lamp (8 W) which was placed in a quartz pipe. The nano-samples were centrifuged and dye concentration was specified by UV–Vis spectrometer.

3 Results and discussion

Scanning electron microscopy was employed for estimation of morphology and particle size of the products.

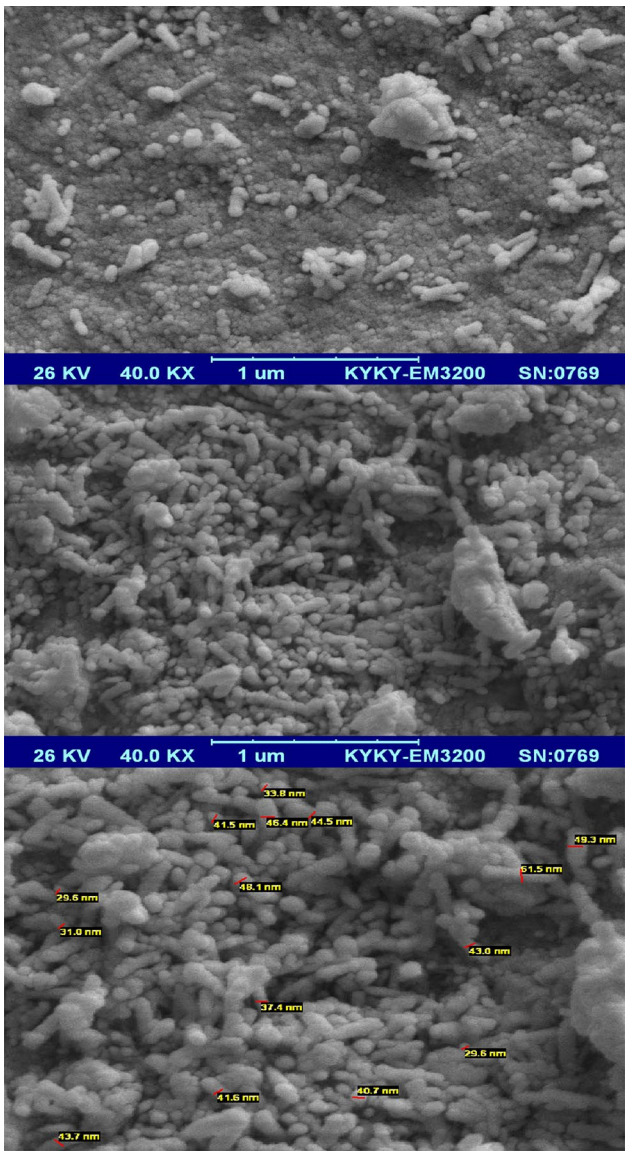

Fig. 2 SEM images of $BaFe_{12}O_{19}$ nanoparticles prepared without using any surfactant and capping agent

Figure 2 shows SEM images of $BaFe_{12}O_{19}$ nanoparticles prepared without using any surfactant and capping agent, results confirm that mono-disperse nanoparticles with average size less than 40 nm were synthesized.

Figure 3 illustrate SEM photograph of barium ferrite nanoparticles synthesized with salicylic acid as a green capping agent, images confirm that mono-disperse nanoparticles with average size around 50 nm were synthesized. Salicylic acid as a neutral surfactant leads to better nucleation in comparison to growth stage.

Gelatin as another green capping agent was used, Fig. 4 illustrates SEM images of $BaFe_{12}O_{19}$ nanoparticles synthesised at presence of Gelatin, it depicts that agglomerated nanoparticles with mediocre size around 100 nm were achieved. It seems that carbohydrate chains remain around the nanoparticles and adsorbed on the surface and at the final bigger particles were obtained.

Polyvinylpyrrolidone as another conventional surface active agent was used and outcomes approve that it is a unsuitable capping agent for preparation of barium ferrite via precipitation method. SEM photograph of barium ferrite nanoparticles synthesised with PVP is illustrated in Fig. 5 which bulk and agglomerated product was obtained.

Figure 6 shows SEM images of $BaFe_{12}O_{19}$ nanostructures synthesised with starch, by applying this safe and cost-effective sugar, mono-disperse nanoparticles with average size less than 35 nm were synthesized.

Concentration effect on the morphology and size of magnetic product was investigated. Figure 7 illustrate SEM photograph of barium ferrite at 200 ml of water, mono disperse nano-rods and rice like product with diameter size about 50 nm was prepared.

Temperature influence on the shape and size was also examined, SEM images of $BaFe_{12}O_{19}$ nanoparticles achieved at 800 °C is shown in Fig. 8, mono-disperse nanoparticles with mediocre size around 50 nm were prepared.

Reaction with salicylic acid was chosen as basic reaction and effect of various parameters on the shape and size was also examined. Calcination temperature influence on the size was investigated. Figure 9 illustrates SEM photograph of barium ferrite nanoparticles calcined at 200 °C.

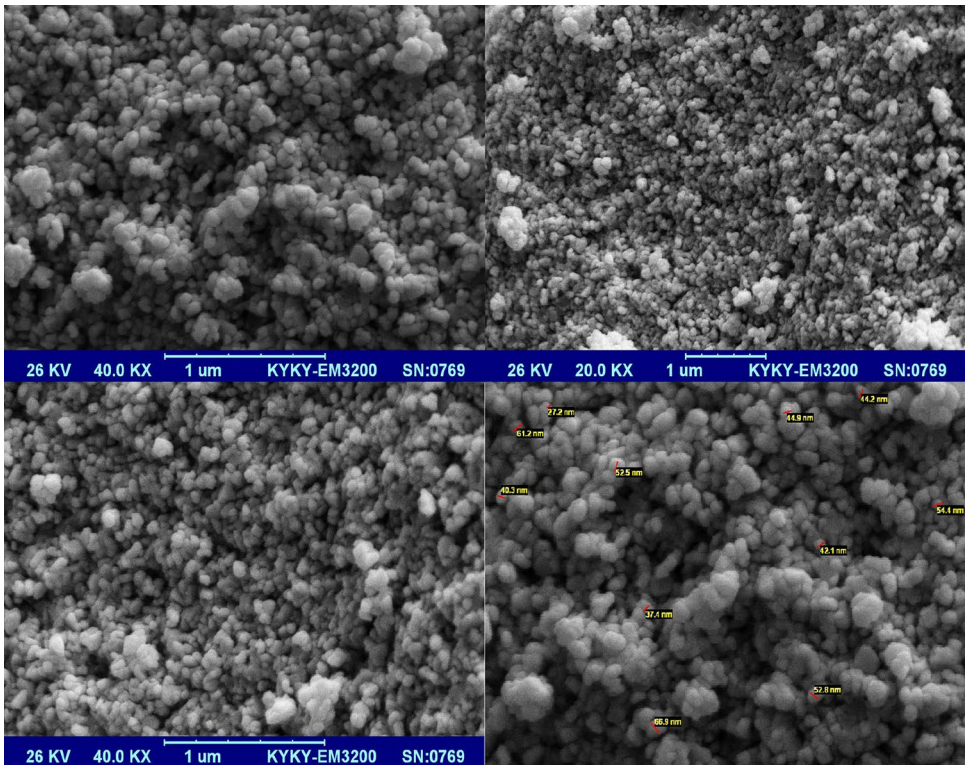

Fig. 3 SEM photograph of barium ferrite nanoparticles synthesised with salicylic acid

Mono-disperse magnetic nanoparticles with size lower than 50 nm was achieved.

SEM images of $BaFe_{12}O_{19}$ nanoparticles calcined at 500 °C are shown in Fig. 10. Mono-disperse nanoparticles around 50 nm were synthesized.

Figure 11 illustrates SEM photographs of titanium dioxide at ethanol nanoparticles that show nanoparticles with size about 50 nm were prepared.

The effect of solvent on the shape was surveyed, SEM images of TiO_2 at methanol (Fig. 12) confirm mono-disperse nano spheres with diameter size about 50 nm were obtained.

Photocatalyst and magnetic nanocomposite is depicted in Fig. 13. SEM images of $BaFe_{12}O_{19}$–TiO_2 (50:50%) nanocomposites approve by adsorption and synthesise of titanium dioxide on the magnetic core, nanoparticles with dimensions less than 100 nm were prepared.

Figure 14 shows the Fourier transform infrared (FT-IR) spectrum of the as-prepared $BaFe_{12}O_{19}$ nanoparticles, the absorptions band at 430, 580 and 619 cm^{-1} are assigned to the stretching mode of Fe–O and Ba–O. The spectrum exhibits broad absorption peak around 3479 cm^{-1}, corresponding to the stretching mode of O–H group of hydroxyl group and the band near 1431 cm^{-1} is assigned to vibration mode of aromatic ring C=C bond due to the adsorption of salicylic acid on the surface of nanoparticles.

FT-IR spectrum of the TiO_2 nanoparticle is shown in Fig. 15 The absorptions band at 345 and 621 cm^{-1} are assigned to the stretching mode of Ti–O bonds. Figure 16 illustrates the FT-IR spectrum of the as-prepared $BaFe_{12}O_{19}$–TiO_2 (50:50%) nanocomposites. Strong

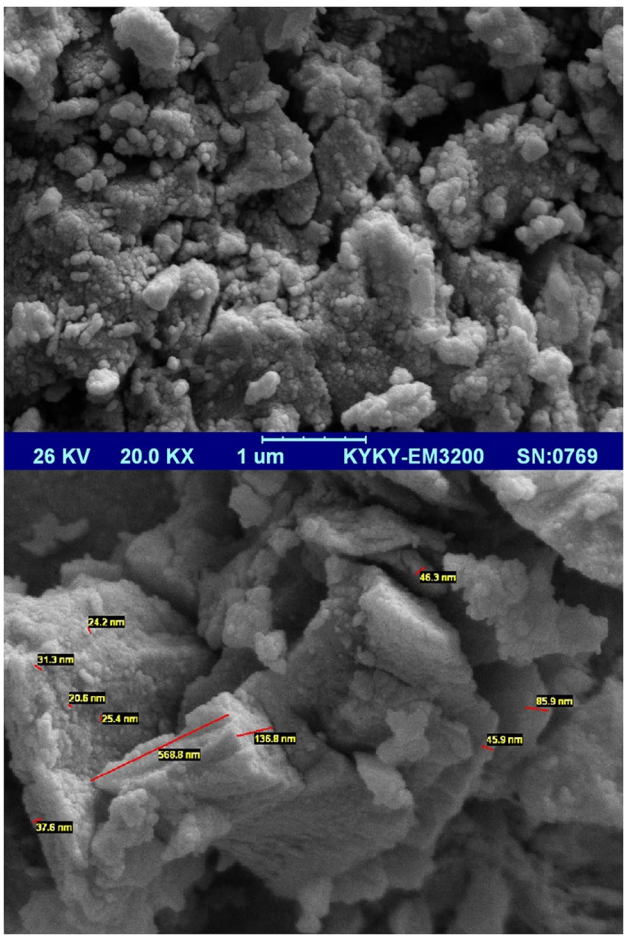

Fig. 4 SEM images of $BaFe_{12}O_{19}$ nanoparticles synthesised in the presence of Gelatin

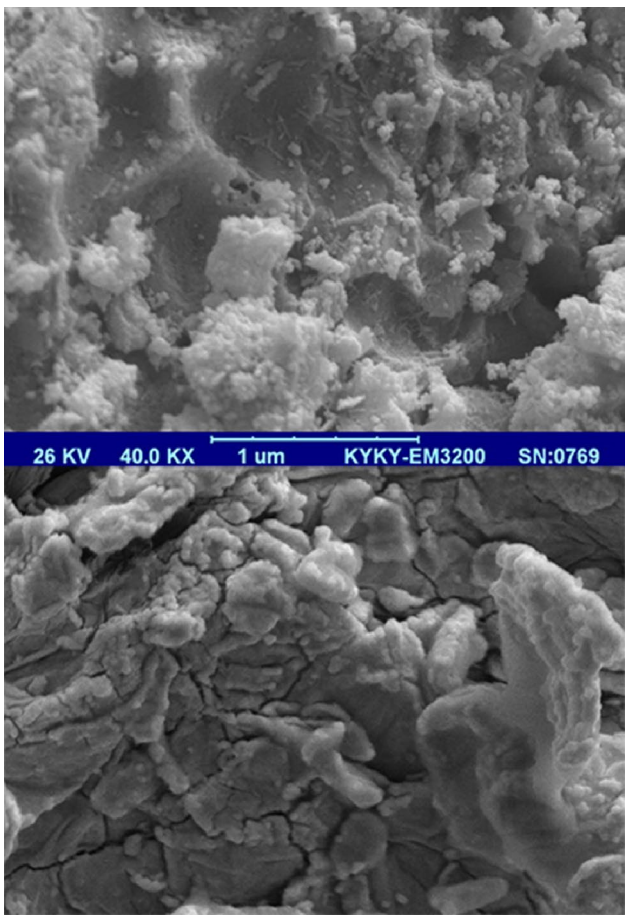

Fig. 5 SEM of barium ferrite nanoparticles synthesised in the presence of PVP

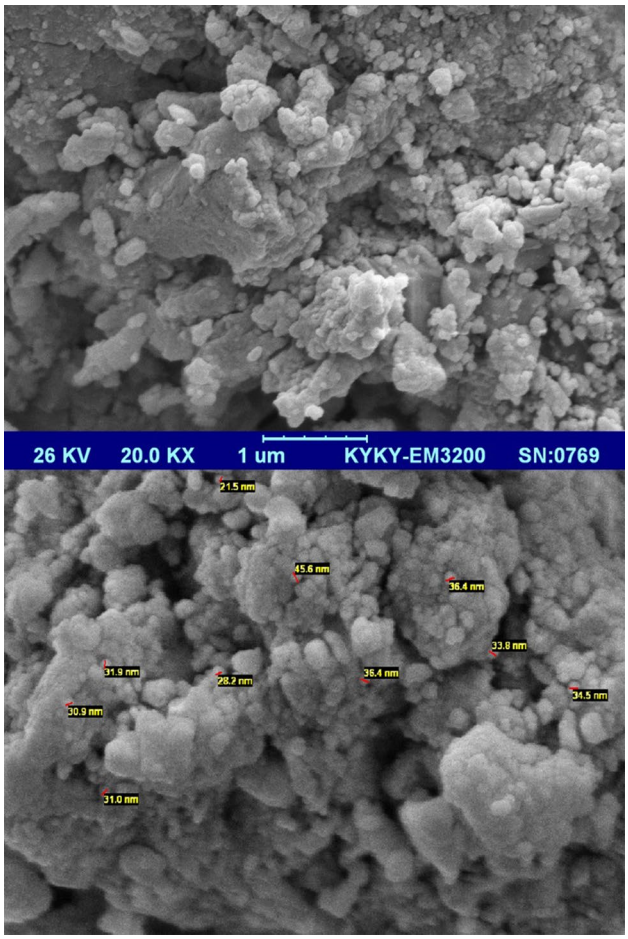

Fig. 6 SEM images of $BaFe_{12}O_{19}$ nanostructures synthesised with starch

absorption band approves presence of magnetic nanoparticles. All absorptions band at 300 and 553 cm^{-1} are assigned to the stretching mode of Fe–O, Ba–O and Ti–O bonds. Absorptions around 3414 cm^{-1} are corresponding to the O–H group.

The structure and composition of the $BaFe_{12}O_{19}$ nanoparticles was investigated. Figure 17 shows XRD pattern of sample including barium ferrite nanoparticles. The XRD pattern of $BaFe_{12}O_{19}$ reveals the typical diffraction pattern of pure Hexagonal phase (JCPDS No.: 07-0276) with *P*63-*mmc* space group which is consistent with pure barium ferrite.

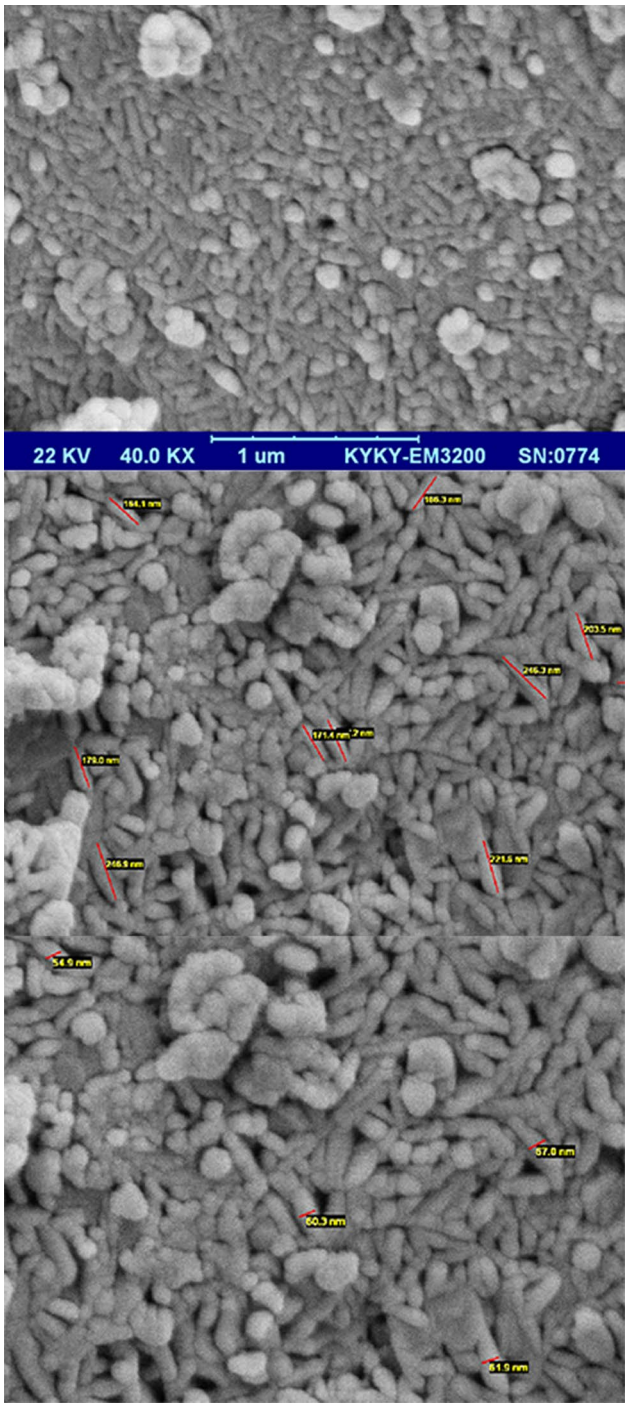

Fig. 7 SEM of barium ferrite nanoparticles prepared at 200 ml of water

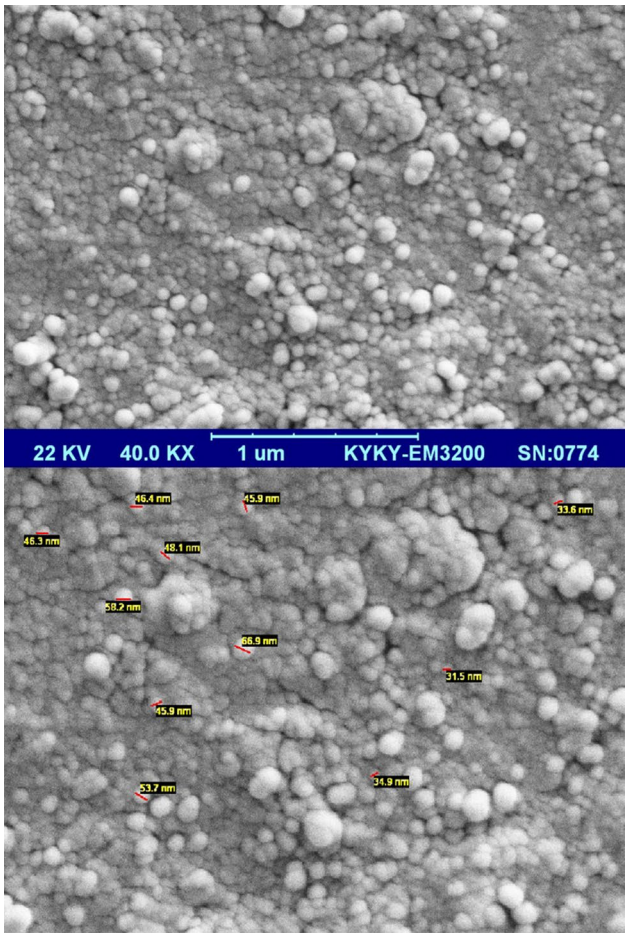

Fig. 8 SEM of $BaFe_{12}O_{19}$ nanoparticles achieved at 800 °C

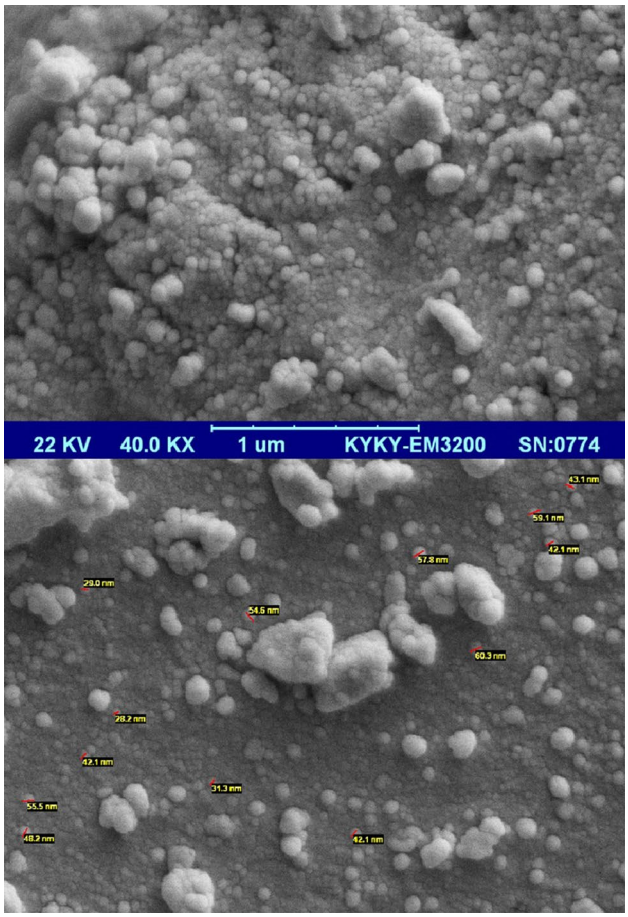

Fig. 9 SEM of barium ferrite nanoparticles calcined at 200 °C

XRD pattern of TiO_2 nanoparticles was also investigated in Fig. 18. Titanium dioxide reveals the typical diffraction pattern of agreement with pure tetragonal TiO_2 phase (JCPDS No.: 02-0387) with *I*41-*amd* and (JCPDS No.:0 1-1292) with *P*42-*mnm* space group which has.

Figure 19 depicts XRD pattern of $BaFe_{12}O_{19}$–TiO_2 (50:50%) nanocomposite. Presence of both hexagonal phase and pure tetragonal phase was confirmed in the XRD pattern.

The crystalline sizes from Scherrer equation, $Dc = K\lambda/\beta Cos\theta$, was calculated, where β is the width of the observed

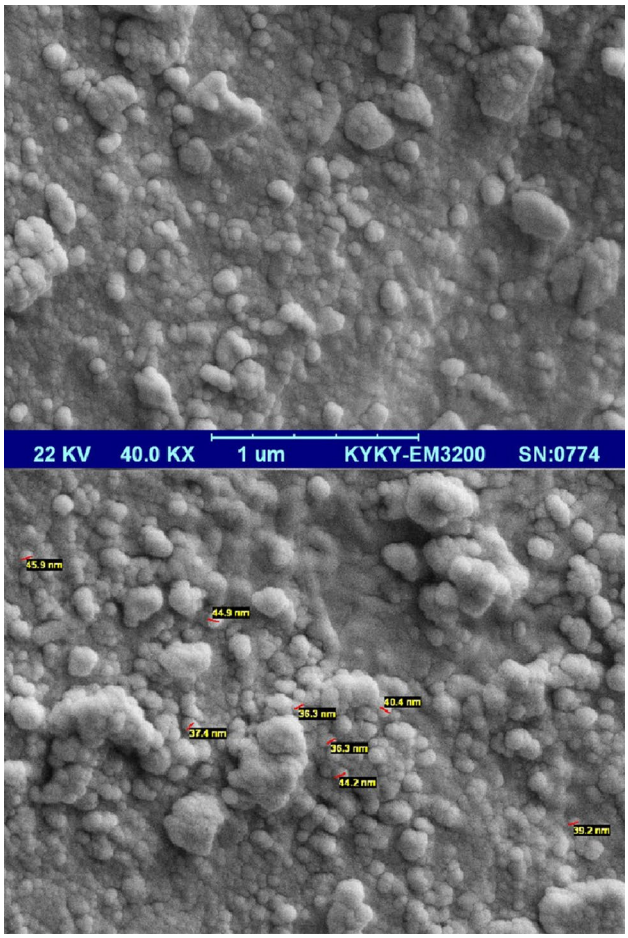

Fig. 10 SEM images of $BaFe_{12}O_{19}$ calcined at 500 °C

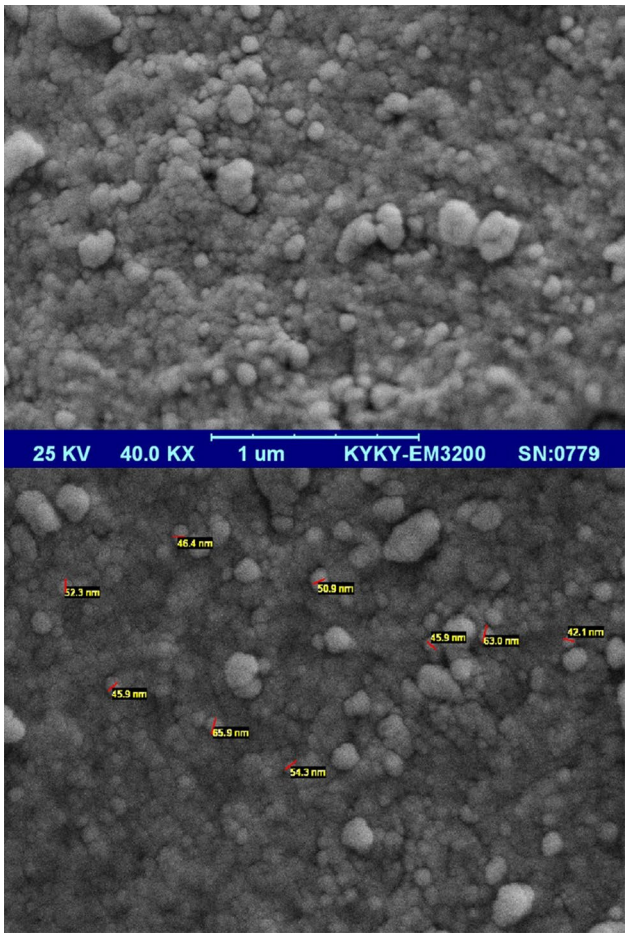

Fig. 11 SEM of TiO_2 prepared at ethanol

diffraction peak at its half maximum intensity (FWHM), K is the shape factor, which takes a value of about 0.9, and λ is the X-ray wavelength (CuKα radiation, equals to 0.154 nm). The average crystalline size for $BaFe_{12}O_{19}$, TiO_2, $BaFe_{12}O_{19}$–TiO_2 (50:50%) nanoparticles were found to be about 19, 21 and 29 nm respectively.

Room temperature magnetic property of ferrite that was prepared by salycilic acid was studied using VSM instrument and is shown in Fig. 20. The result indicates that, the sample exhibit ferromagnetic property. Saturation magnetizations around 36 emu/g and coercivity about 1650 Oe have been achieved.

Figure 21 shows VSM curve of $BaFe_{12}O_{19}$ nanoparticles prepared at diluted solvent (200 ml of water instead of 100 ml), the product show ferromagnetic property. Saturation magnetizations around 45 emu/g and coercivity about 1285 Oe have been achieved.

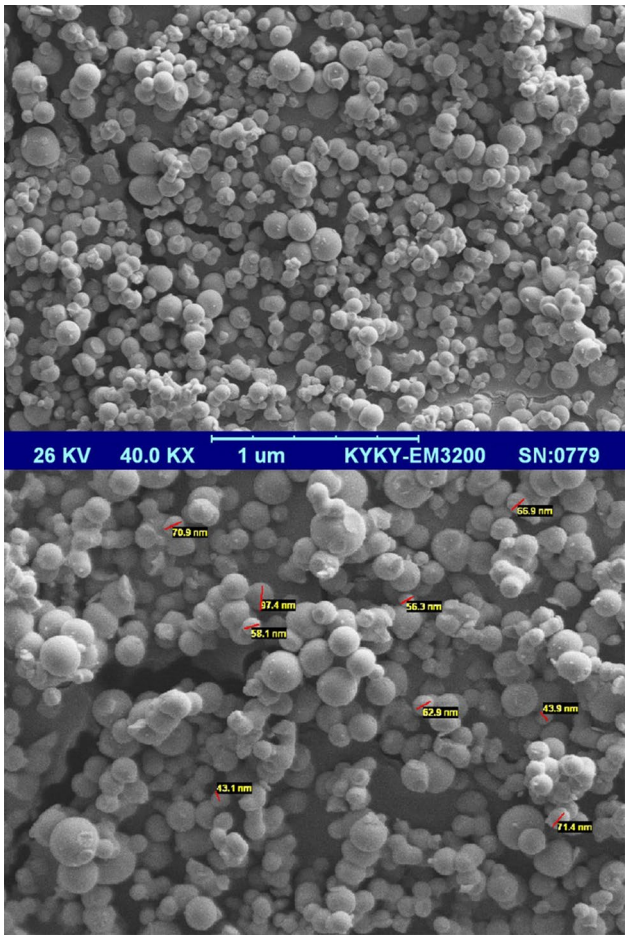

Fig. 12 SEM images of TiO_2 synthesized at methanol

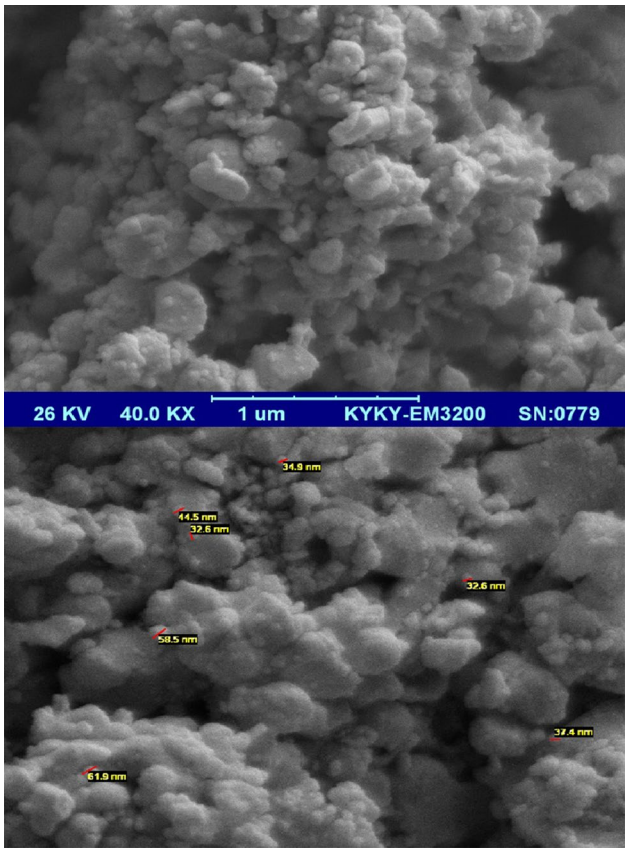

Fig. 13 SEM images of $BaFe_{12}O_{19}$–TiO_2 nanocomposites

Figure 22 depicts magnetization curve of $BaFe_{12}O_{19}$–TiO_2 (50:50%) that also exhibits ferromagnetic behaviour with a coercivity of about 2700 Oe and saturation magnetization of 18 emu/g.

The magnetic property of the prepared nanocomposites is an essential characteristic of a heterogeneous nanocomposite since materials with this magnetic behaviour have low tendency in inter-particles agglomeration caused by dipole–dipole interaction in comparison with ferromagnetic nanocomposites. The results also indicate that nanocomposite formation give rise to coercivity enhancement.

The mechanism of photo-degradation of toxic azo-dyes under ultraviolet irradiation in the presence of titanium

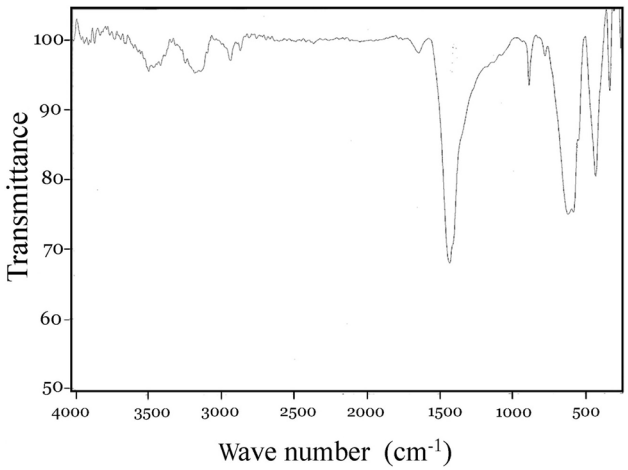

Fig. 14 FT-IR of barium ferrite nanoparticles

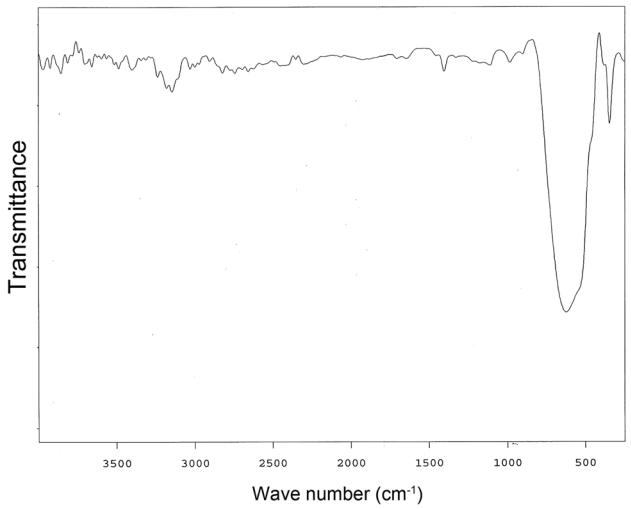

Fig. 15 FT-IR of TiO_2 nanoparticle

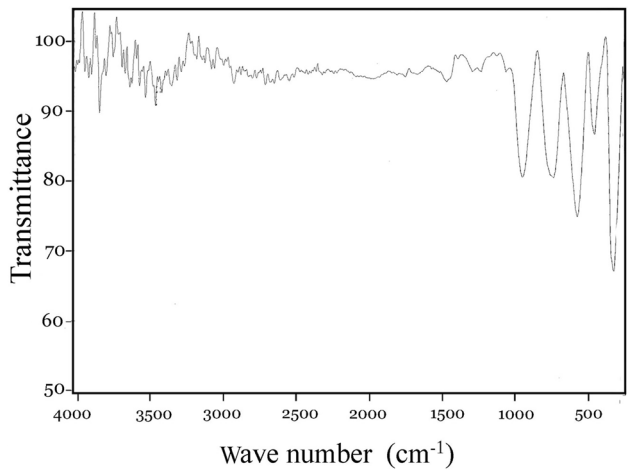

Fig. 16 FT-IR of $BaFe_{12}O_{19}$–TiO_2 nanocomposite

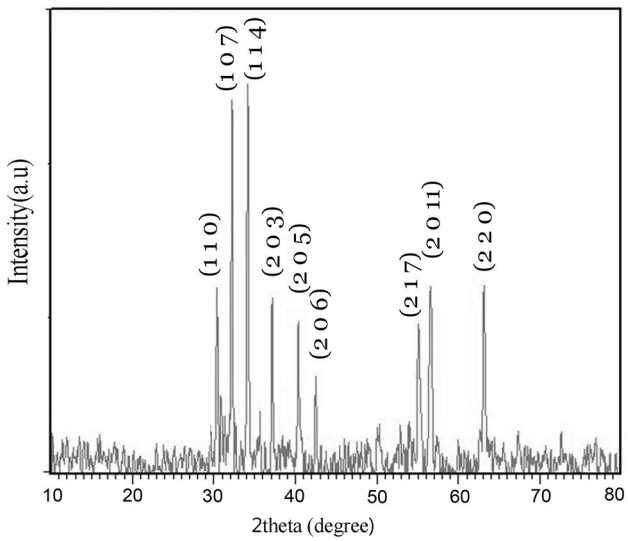

Fig. 17 XRD pattern of $BaFe_{12}O_{19}$ nanoparticles

dioxide as an effective photo-catalyst with an indirect band gap about 3.2 eV is shown in Fig. 23. Acid black, acid blue, acid violet and methyl orange as typical organic pollutants were employed as targets because of the relative stability of their molecular structure. UV–Vis absorption of TiO_2 is shown in Fig. 24 respectively. The as-prepared nanocomposite has the potential to be applied to improve environmental problems associated with organic and toxic water pollutants.

Maximum absorption peaks (λmax) of organic dyes that were used for degradation under UV light are prepared from UV–Vis absorption spectra and were confirmed by scientific literature. The photo-catalytic activity

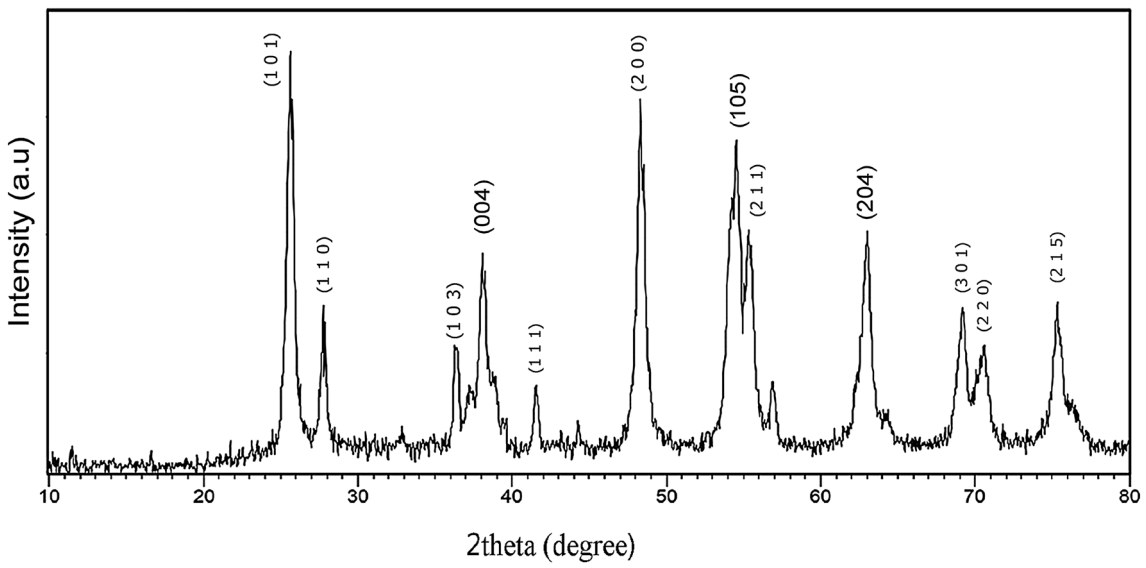

Fig. 18 XRD pattern of TiO_2 nanoparticles

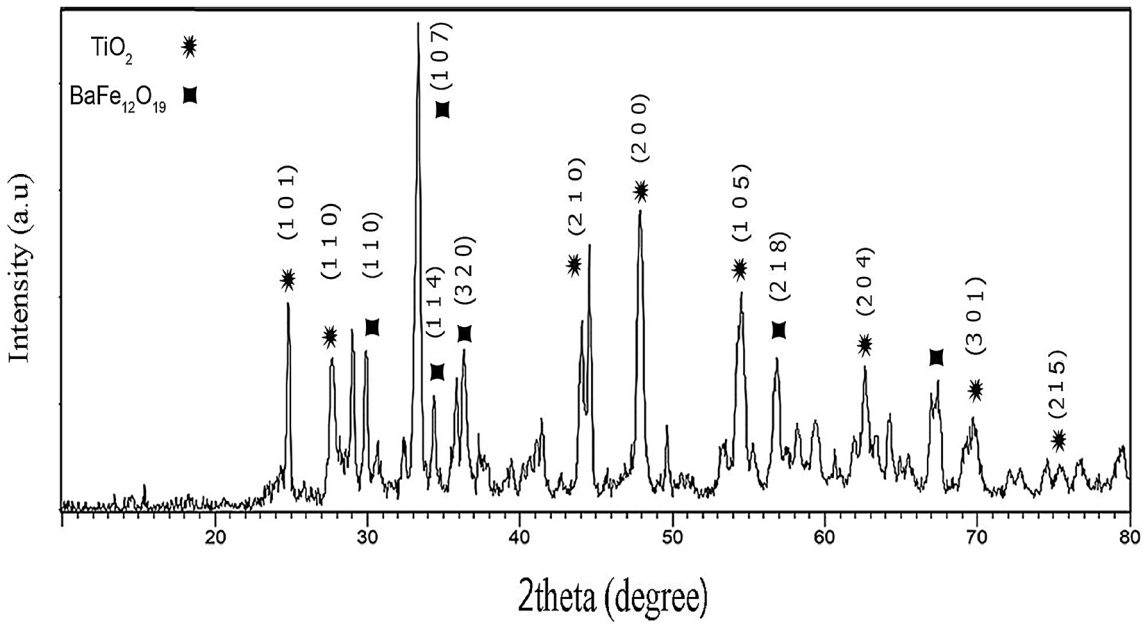

Fig. 19 XRD pattern of $BaFe_{12}O_{19}$–TiO_2 nanocomposite

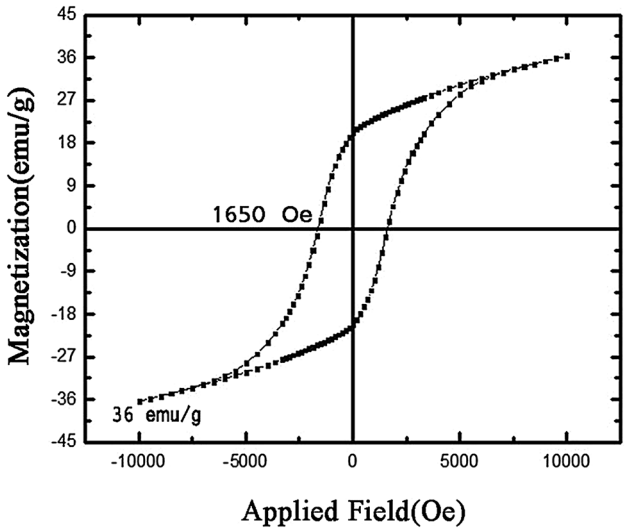

Fig. 20 VSM curve of barium ferrite nanoparticle

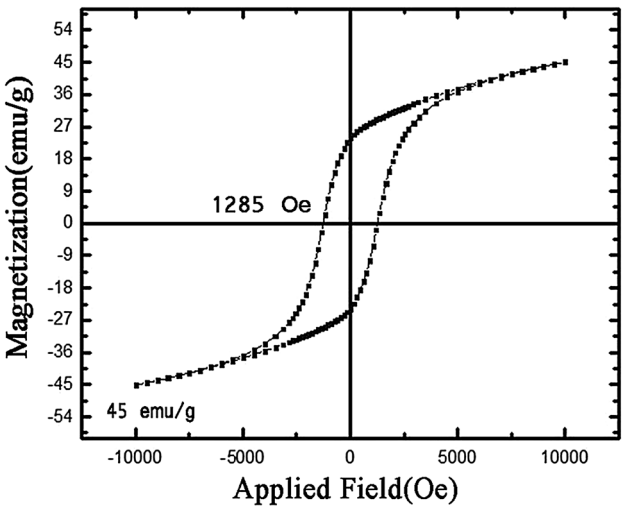

Fig. 21 VSM curve of $BaFe_{12}O_{19}$ nanoparticles prepared at 200 ml of water

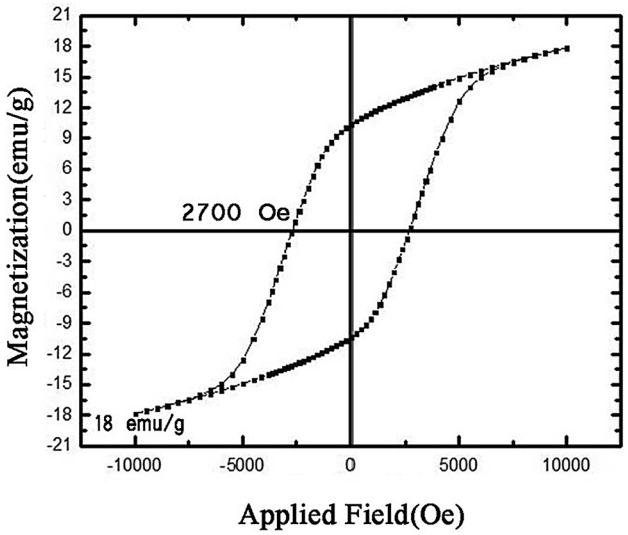

Fig. 22 VSM curve of $BaFe_{12}O_{19}$–TiO_2 (50:50%) nanocomposite

of the nanocomposite was evaluated by monitoring the degradation of organic dyes in an aqueous solution, under UV irradiation. The changes in the concentration of dye are illustrated in Fig. 25 acid blue, acid violet, methyl orange and acid black were degraded at 15, 40, 60 and 30 min respectively by $BaFe_{12}O_{19}$–TiO_2 (50:50%) nanocomposite. As time increase; more and more dyes are adsorbed on the nanoparticles catalyst, until the absorption peaks (λmax) of acid black, methyl orange, and acid blue decrease and vanish around 60 min. The dyes concentration decreased rapidly with increasing UV–irradiation time organic dyes decompose to carbon dioxide, water and other less toxic or nontoxic residuals [10–16].

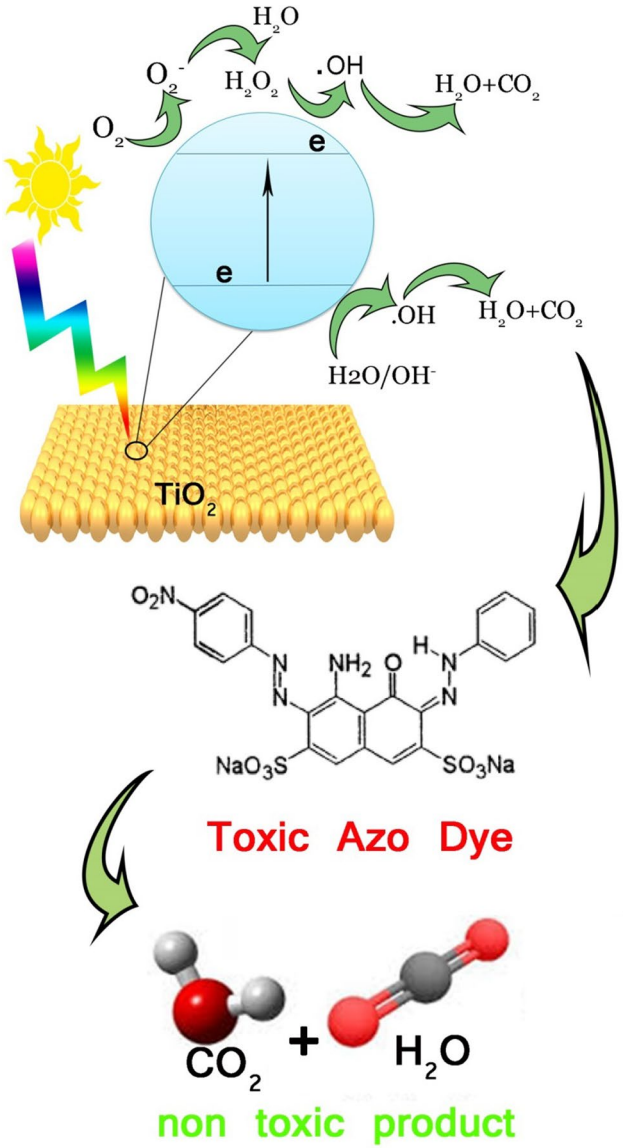

Fig. 23 Photo-catalyst mechanism in degradation of toxic dyes

4 Conclusions

In conclusion synthesis, characterization, and photocatalytic activity of $BaFe_{12}O_{19}$, TiO_2 and $BaFe_{12}O_{19}$–TiO_2 (50:50%) nanocomposite were reported. VSM confirmed that nanoparticles and nanocomposite exhibit ferromagnetic behaviour. The photocatalytic behaviour of $BaFe_{12}O_{19}$–TiO_2 (50:50%) nanocomposite was evaluated using the degradation of four various azo dyes under UV light irradiation. The results show that precipitation method is a suitable method for preparation of $BaFe_{12}O_{19}$–TiO_2 (50:50%) nanocomposites as a candidate for photocatalytic applications.

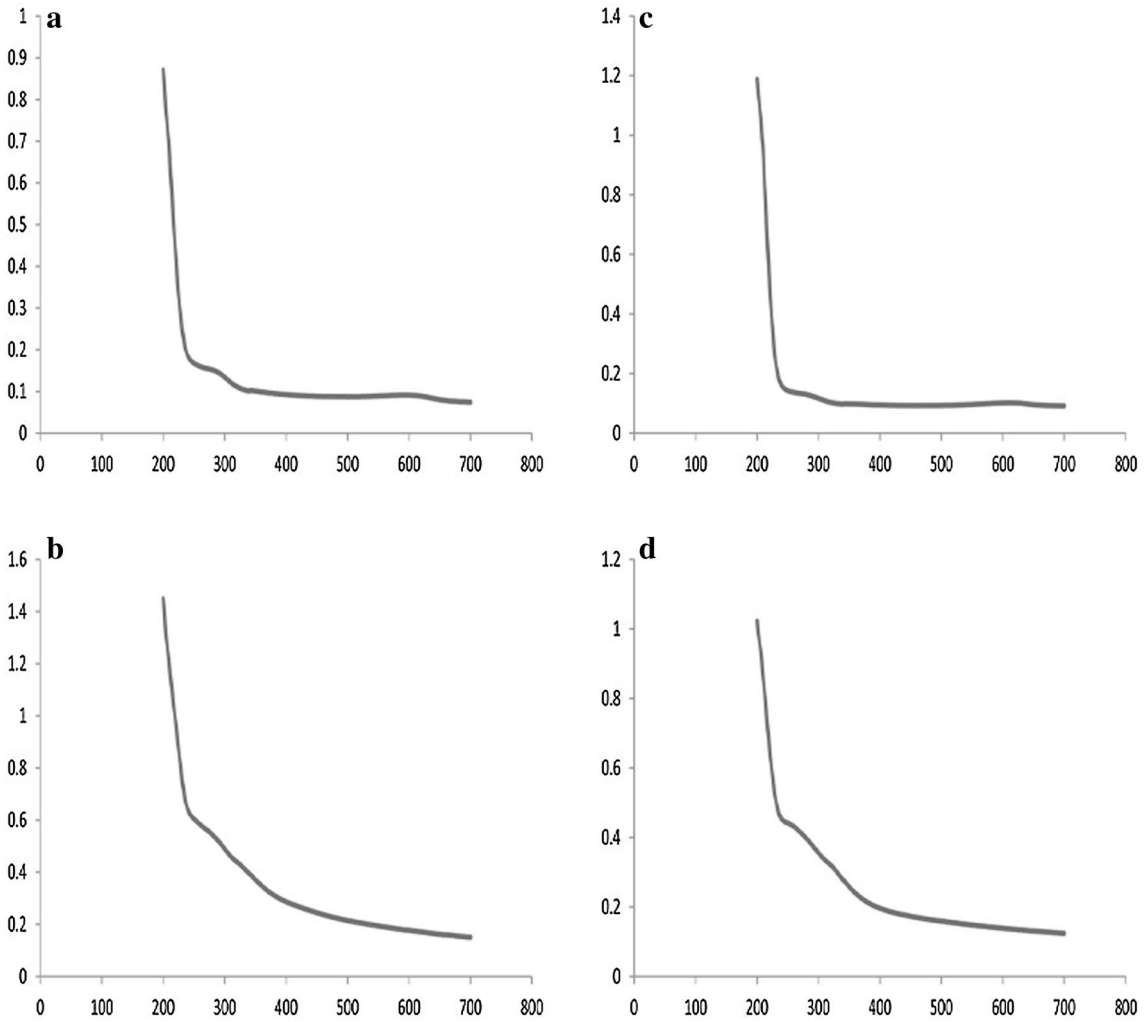

Fig. 24 UV–Vis absorption of dyes in the presence of $BaFe_{12}O_{19}$–TiO_2 (50:50%) nanocomposite photocatalyst **a** acid blue, **b** acid black, **c** acid violet, **d** methyl orange

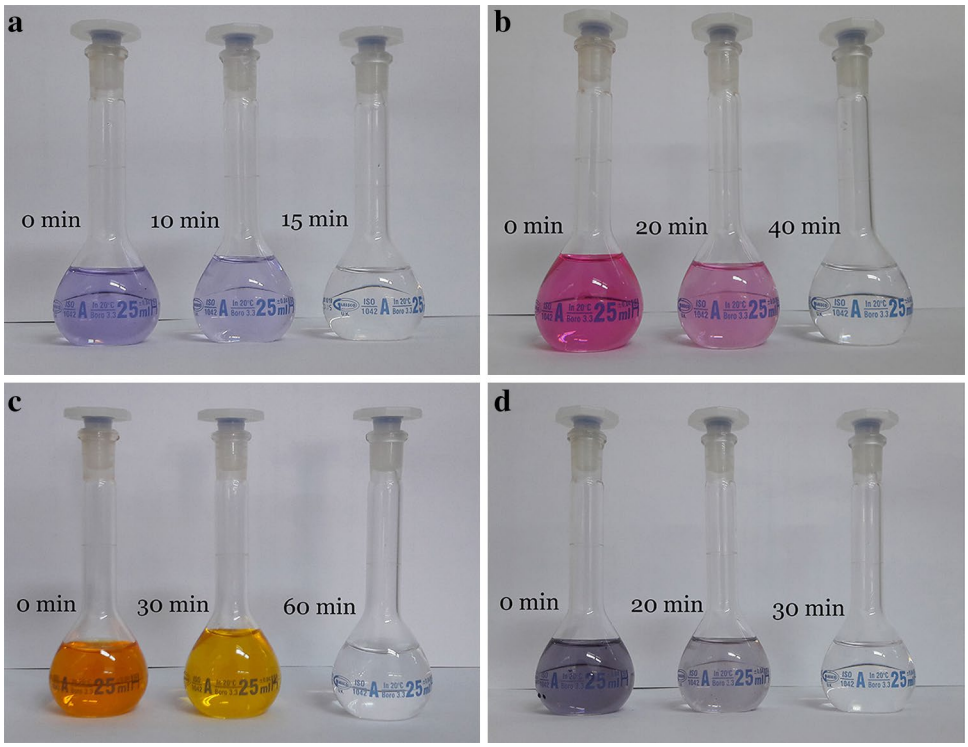

Fig. 25 Photo-degradation of **a** acid blue, **b** acid violet, **c** methyl orange, **d** acid black by $BaFe_{12}O_{19}$–TiO_2 (50:50%) nanocomposite

References

1. T. Gonzalez-Carreno, M.P. Morales, C.J. Serna, Mater. Lett. **43**, 97 (2000)
2. Z. Haijun, L. Zhichao, M. Chengliang, X. Yao, Z. Liangying, W. Mingzhong, Mater. Sci. Eng. B **96**, 289 (2002)
3. X. Liu, J. Wang, L.-M. Gan, S.-C. Ng, J. Magn. Magn. Mater. **195**, 452 (1999)
4. G. Mu, C. Na, P. Xifeng, S. Haigen, M. Gu, Mater. Lett. **62**, 840 (2008)
5. H. Zhang, Z. Liu, C. Ma, X. Yao, L. Zhang, M. Wu, Mater. Chem. Phys. **80**, 129 (2003)
6. S.E. Jacobo, C. Domingo-Pascual, R. Rodriguez-Clemente, M.A. Blesa, J. Mater. Sci. **32**, 1025 (1997)
7. N. Koga, T. Tsutaoka, J. Magn. Magn. Mater. **313**, 168 (2007)
8. K.M. Reddy, V.M. Sunkara, A.R. Reddy, Mater. Chem. Phys. **78**, 239 (2003)
9. R.S. Sonawane, S.G. Hegde, M.K. Dongare, Mater. Chem. Phys. **77**, 744 (2003)
10. D. Ghanbari, S. Sharifi, A. Naraghi, G. Nabiyouni, J. Mater. Sci. Mater. Electron. **27**, 5315 (2016)
11. A. Shabani, G. Nabiyouni, J. Saffari, D. Ghanbari, J. Mater. Sci. Mater. Electron. **27**, 8661 (2016)
12. S. Masoumi, G. Nabiyouni, D. Ghanbari, J. Mater. Sci. Mater. Electron. **27**, 9962 (2016)
13. S. Masoumi, G. Nabiyouni, D. Ghanbari, J. Mater. Sci. Mater. Electron. **27**, 11017 (2016)
14. G. Rezaei, G. Nabiyouni, D. Ghanbari, J. Mater. Sci. Mater. Electron. **27**, 11339 (2016)
15. K. Hedayati, M. Goodarzi, M. Kord, Main Group Met. Chem. **39**, 183 (2016)
16. K. Hedayati, M. Kord, M. Goudarzi, D. Ghanbari, S. Gharigh, J. Mater. Sci. Mater. Electron. **28**, 1577 (2017)